Received: 31 March 2020 | Revised: 20 July 2020 | Accepted: 27 July 2020

DOI: 10.1002/mgg3.1489

Molecular Genetics & Genomic Medicine Open Access WILEY

ORIGINAL ARTICLE

Characterization of *CRB1* splicing in retinal organoids derived from a patient with adult-onset rod-cone dystrophy caused by the c.1892A>G and c.2548G>A variants

Xiao Zhang[1,2] | **Jennifer A. Thompson**[3] | **Dan Zhang**[2] | **Jason Charng**[2] | **Sukanya Arunachalam**[2] | **Terri L. McLaren**[1,3] | **Tina M. Lamey**[1,3] | **John N. De Roach**[1,3] | **Luke Jennings**[2] | **Samuel McLenachan**[1,2] | **Fred K. Chen**[1,2,3,4,5]

[1]Centre for Ophthalmology and Visual Science, The University of Western Australia, Nedlands, WA, Australia

[2]Lions Eye Institute, Nedlands, WA, Australia

[3]Australian Inherited Retinal Disease Registry and DNA Bank, Sir Charles Gairdner Hospital, Nedlands, WA, Australia

[4]Department of Ophthalmology, Royal Perth Hospital, Perth, WA, Australia

[5]Department of Ophthalmology, Perth Children's Hospital, Nedlands, WA, Australia

Correspondence
Samuel McLenachan, Lions Eye Institute, 2 Verdun Street, Nedlands, Western Australia 6009 Australia.
Email: smclenachan@lei.org.au

Funding information
Saleeba family; Retina Australia; The University of Western Australia, Grant/Award Number: International Postgraduate Research Scholarship; The Ophthalmic Research Institute of Australia; Australian Foundation for the Prevention of Blindness; National Health and Medical Research Council, Grant/Award Number: GNT1116360, GNT1188694 and MRF1142962; Miocevich family; McCusker family

Abstract

Background: Mutations in the human crumbs homologue 1 (*CRB1*) gene are associated with a spectrum of inherited retinal diseases. However, functional studies demonstrating the impact of individual *CRB1* mutations on gene expression are lacking for most variants. Here, we investigated the effect of two *CRB1* variants on pre-mRNA splicing using neural retinal organoids (NRO) derived from a patient with recessive rod-cone dystrophy caused by compound heterozygous mutations in *CRB1* (c.1892A>G and c.2548G>A).

Methods: The patient received ophthalmological examinations including multimodal imaging. NRO were differentiated from induced pluripotent stem cells (iPSCs) derived from the patient and a control subject. *CRB1* transcripts were characterized by RT-PCR and Sanger sequencing.

Results: The Patient displayed retinal thickening with disorganization of retinal layers and preservation of para-arteriolar retinal pigment epithelium. Both patient and control iPSC produced NRO containing photoreceptor progenitor cells expressing *CRB1* mRNA. Patient NRO expressed a novel *CRB1* transcript displaying skipping of exon 6. *CRB1* transcripts containing the c.2548G>A substitution in exon 7 were expressed in patient NRO.

Conclusions: Together, these results confirm the pathogenicity of the c.1892A>G and c.2548G>A *CRB1* variants in a family with recessive adult-onset rod-cone dystrophy and further demonstrate the effects of these variants on pre-mRNA splicing. This data provide important insights into the pathogenic mechanisms associated with these variants.

KEYWORDS

CRB1, crumbs complex, retinal organoids, retinitis pigmentosa, splicing

1 | INTRODUCTION

Mutations in the human crumbs homolog-1 (*CRB1*, OMIM#604210, NM_201253.2) gene are associated with a spectrum of inherited retinal diseases (IRD), including Leber congenital amaurosis 8 (LCA8), retinitis pigmentosa 12 (RP12), rod-cone dystrophy of varying age of onset, and foveal retinoschisis of adult onset (Bujakowska et al., 2012; den Hollander et al., 2001). These distinct phenotypes share the common features of photoreceptor and retinal pigment epithelium (RPE) degeneration with variable vascular abnormalities in the peripheral retina. Unique clinical features specifically found in *CRB1*-associated retinopathy are preservation of the para-arteriolar RPE (den Hollander et al., 2000), retinal telangiectasia with exudation (also referred to as Coats-like vasculopathy), as well as thickening of the retina and disorganized retinal layering (Jacobson et al., 2003).

The Genome Aggregation Database (gnomAD) currently lists 1833 known variants for the human *CRB1* gene, including 910 missense substitutions, 317 synonymous substitutions, 109 3'/5'-UTR variants, 60 splice variants, 26 frameshifting mutations, 9 indels, 30 nonsense mutations, 371 intronic sequence variants and 1 start site mutation. Despite this significant progress in the identification of *CRB1* gene variants, the pathogenicity of many of these variants remains unclear. A total of 323 disease-causing *CRB1* variants are currently listed in the Human Genome Mutation Database (Stenson et al., 2017). In the absence of functional evidence, the clinical interpretation of these variants is somewhat influenced by *in silico* predictions according to American College of Medical Genetics and Genomics and Association for Molecular Pathology (ACMGG/AMP) guidelines (Richards, et al., 2015). While these *in silico* programs provide an excellent tool for predicting the clinical significance of novel gene variants, classifications obtained must be treated with caution until functional molecular evidence becomes available. With the ever-expanding catalogue of known variants in *CRB1* and other disease-causing genes, it is essential that the effects of these mutations are established through molecular analyses. A clear understanding of the underlying mechanisms by which mutations exert their pathogenic effects can also inform genotype-phenotype correlations and guide future development of potential therapies.

Until recently, molecular characterization of IRD-causing mutations has been limited by a paucity of available retinal tissues from affected patients for analysis. Since many IRD genes are expressed specifically in the retina, access to patient retinal cells is essential for the characterization of IRD mutations at the RNA and protein level in the context of the affected cell type. The discovery of methods for the generation of induced pluripotent stem cells (iPSCs) from human somatic cells has provided the means for generating retinal cells from patients carrying disease-causing mutations in IRD genes (Chen et al., 2014). Recently, we reported the generation of iPSC lines from a patient with rod-cone dystrophy caused by compound heterozygous mutations (c.1892A>G and c.2548G>A) in *CRB1* (Zhang et al., 2018). Interestingly, the c.1892A>G variant has been associated with a milder clinical phenotype (onset ≥10 years). In this study, we provide a detailed description of this patient's clinical phenotype and investigate the consequence of their mutations on transcript splicing using the patient's iPSC-derived retinal tissues.

2 | METHODS

Both clinical and experimental aspects of this study were approved by the University of Western Australia (RA/4/1/7916, RA/4/20/5717) and the Sir Charles Gairdner Hospital (2001-053) Human Research Ethics Committees. Written consent was obtained from the patient and all procedures were carried out in accordance with the requirements of the National Health & Medical Research Council of Australia and the Declaration of Helsinki.

2.1 | Clinical assessment

History and full ophthalmic examination including best-corrected visual acuity using the Early Treatment of Diabetic Retinopathy Study (ETDRS) letter chart and dilated fundus examination was undertaken. Multimodal retinal imaging included ultra-wide-field color fundus photography, green-light autofluorescence (AF) imaging (P200Tx and California, Optos plc, Dunfermline, UK), 30° and 55° scanning laser ophthalmoscopy including near-infrared reflectance (NIR), blue-light and near-infrared AF and spectral domain optical coherence tomography (SD-OCT, Spectralis OCT2 and Spectralis HRA2, Heidelberg Engineering, Heidelberg, Germany).

2.2 | Genetic analysis and interpretation

Genetic analysis utilized genomic DNA extracted from peripheral blood samples collected and stored as detailed previously (Paterson et al., 2012). Analysis of proband genomic DNA targeted known variants in 28 genes associated with autosomal recessive retinitis pigmentosa (ARRP) using the Apex ARRP Array (version 5.3; performed by Asper Ophthalmics, Tartu, ESTONIA) coupled with haplotype analysis to exclude non-candidate genes (performed by the Australian Genome Research Facility (AGRF), Brisbane, Australia), as described previously (Paterson

et al., 2012). Bidirectional Sanger sequencing of coding and flanking intronic regions of candidate genes *CRB1*, *PDE6A*, and *RPE65* was performed on DNA of the proband and an affected sibling to detect novel candidate variants in these genes. The phase of *CRB1* variants was established in parental DNA, and their presence in two siblings was ascertained by bidirectional Sanger sequencing (performed by ASPER Ophthalmics or AGRF). Variant nomenclature is in accordance with recommendations of the Human Genome Variation Society (den Dunnen et al., 2016unnen et al., 2016), with sequencing results aligned to the *CRB1* reference sequence NM_201253.2 (OMIM#604210). Nucleotide 1 corresponds to the A of the ATG initiation codon.

Variant pathogenicity assessment encompassed *in silico* pathogenicity predictions, allele frequencies sourced from gnomAD (Karczewski et al., 2020), data from variation databases (LOVD/ClinVar/dbSNP) and the scientific literature, and the clinical diagnosis. *In silico* pathogenicity assessment utilized Mutation Taster (Schwarz, Rodelsperger, Schuelke, & Seelow, 2010), SIFT (Ng & Henikoff, 2001), PolyPhen2 (Adzhubei et al., 2010), Align GVGD (Tavtigian, Byrnes, Goldgar, & Thomas, 2008), REVEL (Ioannidis et al., 2016), M-CAP (Jagadeesh et al., 2016) and the Alamut Visual splicing prediction module (Version 2.11; Interactive Biosoftware). Pathogenicity interpretation was performed in accordance with ACMGG/AMP guidelines (Richards et al., 2015). Additionally, *in silico* splicing analyses were performed using Human Splicing Finder, Version 3.1 (Desmet et al., 2009) and EX-SKIP (Raponi et al., 2011).

2.3 | Cell culture and differentiation

Patient iPSC (LEIi006-A) and the normal control iPSC line (Cat#A18945, Thermo Fisher Scientific) were cultured in feeder-free conditions, on geltrex (Thermo Fisher) coated culture plates in mTeSR1 medium (StemCell Technologies), as previously described (Zhang et al., 2018). The mutations found in peripheral blood DNA were also confirmed in these patient-derived iPSC lines. For directed differentiation into neural retinal organoids (NRO) we followed a previously published protocol (Mellough et al., 2015, 2019). Patient and control iPSC colonies were dissociated into small pieces by EDTA buffer (0.5 mM EDTA and 30 mM NaCl in DPBS ($-Ca^{++}$, $-Mg^{++}$) and then cultured in the DMEM/F-12 medium (Thermo Fisher) with decreasing concentrations of KnockOut Serum Replacement (KOSR, Thermo Fisher) (20% for the first 5 days, 15% until day 12, 10% until day 35) containing MEM Non-Essential Amino Acids Solution (NEAA; Thermo Fisher), B27 (Thermo Fisher) and IGF-1 (StemCell).

2.4 | Transcript analysis

Total mRNA was isolated from early (day 35) NRO using TRIZOL and cDNA was synthesized using the RT^2 First Strand Kit (Qiagen, Hilden, Germany) according to the manufacturer's instructions. Partial cDNA sequences were amplified with Q5 High-Fidelity Polymerase (New England Biolabs, Ipswich, Massachusetts, USA) using primers targeting exons 3–7 or exons 7–8. Primer sequences are listed in Table S1. PCR products were resolved on a 2% agarose gel. The 50 bp DNA Ladder (New England BioLabs) was used as a molecular size marker. Gels were imaged using the ChemiDoc XRS+imaging system (BioRad). After purification with the Gel Purification and PCR Clean-up System (Promega), PCR fragments were assessed by Sanger sequencing (AGRF).

2.5 | Immunostaining analysis

Retinal organoids were fixed with 4% paraformaldehyde, washed, then permeabilized using phosphate-buffered saline (PBS) with 0.1% Triton X-100 for 15 min. The samples were then incubated in 5% BSA in PBS for 1 hr at room temperature. Primary antibodies were applied at 4°C overnight. Secondary antibodies were applied for 2 hours at room temperature. Nuclei were stained with DAPI. The following primary antibodies were used in this study: Mouse anti-Pax6 (1:100, Abcam, AB78545), Rabbit anti-Recoverin (1:200, Merck, AB5585). Secondary antibodies used in this study included Alexa Fluor 546 Goat anti-mouse IgG (1:500, Molecular Probes, A-11003), and Alexa Fluor 546 Goat anti-rabbit IgG (1:500, Molecular Probes, A-11035).

2.6 | Transmission electron microscopy (TEM) analysis

Retinal organoids were fixed in 4% paraformaldehyde, 2% glutaraldehyde in 0.1 M phosphate buffer, pH 7.4. After 24 hours, they were post-fixed in 1% osmium tetroxide in the same buffer for 6 minutes (2 minutes on, 2 minutes off and 2 minutes on) with biowave (PELCO). Samples were then dehydrated in a graded series of ethanol and acetone followed by embedding in resin containing Procure 812, Araldite 502, DDSA and BDMA. Ultrathin (100 nm) sections were prepared and examined with a JEM2100 electron microscope (JEOL).

2.7 | Quantitative PCR

Total mRNA was isolated from NRO cultures using TRIZOL and cDNA was synthesized using the RT^2 First Strand Kit

(Qiagen). Quantitative PCR (qPCR) was performed using RT^2 SYBR Green qPCR Mastermix (Qiagen) and the CFX Connect Real-Time System (BioRad). Data were analyzed using the ΔΔCT method. Gene expression values were normalized to expression levels measured in LEIi005-A iPSC. Sequences for primers used in this study are listed in Table S1.

3 | RESULTS

3.1 | Clinical presentation

The patient was a 50-year-old female initially diagnosed with rod-cone dystrophy and macular cysts at the age of 21. Her presenting Snellen visual acuity was 20/30 in both eyes. Fundus examination in the early stages of the disease showed bilateral cystoid maculopathy with numerous white dots in the periphery resembling fundus albipunctatus. Over the 30 years of follow-up, her vision declined to perception of light in both eyes and the majority of the retina was replaced by heavy intraretinal pigmentation sparing the para-arteriolar regions in the periphery (Figure 1a-b). There was gross thickening of the retina due to disorganized retinal layering (Figure 1c). She also developed non-visually significant posterior subcapsular cataract at age 46.

The proband's brother presented at age 18 with a visual acuity of 20/40 in both eyes and peripheral retinal schisis that led to an initial clinical diagnosis of Goldman-Favre syndrome. He had bilateral cataract extraction at the age of 36, and 9 years later, his vision was reduced to perception of light. He also had heavy intraretinal pigmentation with para-arteriolar sparing (Figure 1d-e) and thickened retina (Figure 1f). Neither the proband nor the affected sibling manifested variable vascular abnormalities or retinal telangiectasia with exudation. The proband's parents underwent similar clinical examinations, with no retinal abnormalities detected (data not shown).

3.2 | Genetic analysis and pathogenicity assessment

Proband DNA was analyzed by Apex ARRP Array, coupled with haplotype analysis to further identify candidate genes. Subsequent Sanger sequencing of *PDE6A* and *RPE65* excluded novel candidate variants in these genes. Two variants in *CRB1* were identified: c.1892A>G and c.2548G>A. Segregation analysis confirmed the paternal (former) and maternal (latter) origin of these variants and their segregation with disease (Figure 2a). These missense variants had predicted amino acid substitutions p.(Tyr631Cys) and

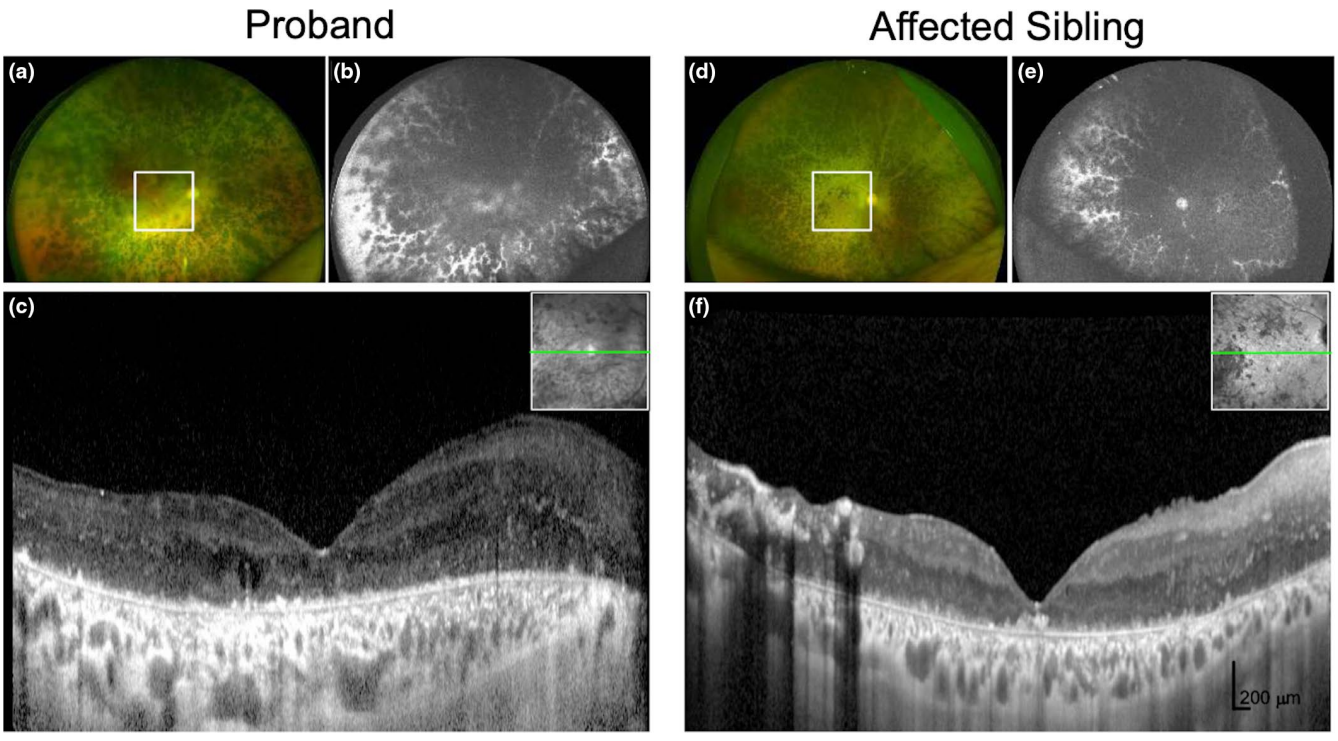

FIGURE 1 (a) Widefield color photography and (b) autofluorescence imaging of the proband's right eye at age 50 shows diffuse retinal pigmentation and para-arteriolar sparing. The square outlines the macular region which was further assessed with OCT. (c) Horizontal OCT scan of the right eye shows thickened retina, disorganized retinal layering with attenuated retinal pigment epithelial layer in the macula region (inset) in the proband. (d-f) Similar features are present in the proband's younger brother at age 46. Scale bar =200 µm.

p.(Gly850Ser), respectively, expected to affect conserved laminin A/G-like domains (Figure 2b).

In silico pathogenicity analysis provided conflicting results for c.1892A>G: despite aberrant splicing predictions, Mutation Taster returned a benign prediction, as did SIFT, PolyPhen 2 and REVEL. AlignGVGD and M-CAP returned a possibly pathogenic result, and EX-SKIP predicted the mutant allele was more likely to cause exon skipping than the wild-type allele. Analysis of this variant using Human Splicing Finder (HSF, version 3.1) predicted potential alteration of splicing due to the introduction of an exonic splice silencer (ESS) site and a cryptic donor splice site (DSS) in exon 6 (Figure S1). Comparison of normal and c.1892A>G *CRB1* splice site sequences in exon 6 revealed the cryptic DSS present in the mutant sequence had a lower HSF score (67.55) than the natural DSS (94.75), suggesting it may not be a strong competitor for the natural DSS. The strength of the Fas-ESS hexamer sequence generated by the c.1892A>G variant could not be assessed by the HSF software, but may promote skipping of exon 6 during pre-mRNA splicing. Interrogation of variation databases and the literature indicated that this variant is rare (allele frequency = 0.000008), and is reported as causative for autosomal recessive retinal dystrophy or retinitis pigmentosa (Hettinga, van Genderen, Wieringa, Ossewaarde-van Norel, & de Boer, 2016; Talib et al., 2017). Recent reports have additionally provided *in vitro* evidence of mislocalized CRB1 protein and misplaced photoreceptors in patient-derived retinal organoids subsequent to this variant occurring in *trans* with a nonsense *CRB1* variant (Quinn et al., 2019). The scientific literature, thus, suggests a pathogenic status for this variant.

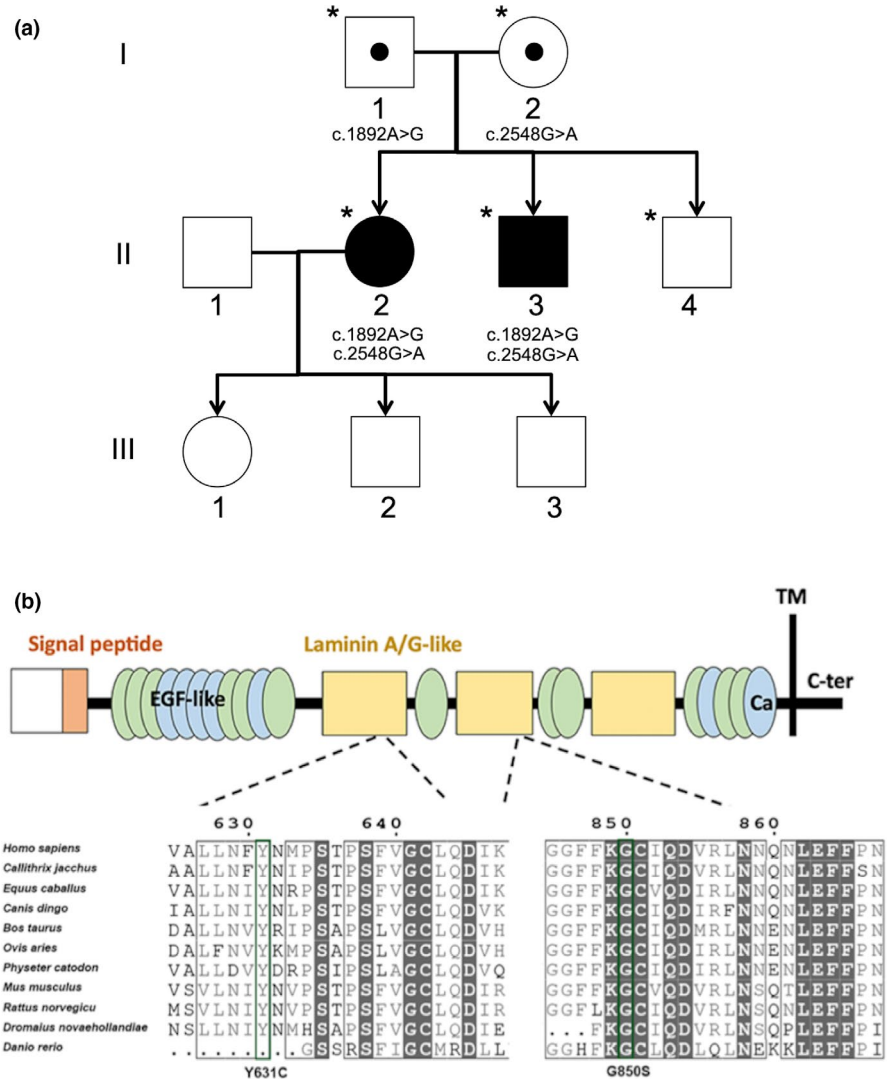

FIGURE 2 (a) The family pedigree shows a recessive inheritance pattern with the proband (II:2) and her affected brother (II:3) having inherited the c.1892A>G variant from their carrier father and the c.2548G>A variant from their carrier mother. (b) These variants, localized to the conserved laminin A/G-like domains, are predicted to result in p.(Tyr631Cys) and p.(Gly850Ser), respectively. Orange, signal peptide; green, EGF-like domain; blue, EGF-like calcium-binding domain; yellow, Laminin A/G-like domain. TM, transmembrane; C-ter, C-terminal.

In contrast, the c.2548G>A variant was predicted to be pathogenic by all *in silico* algorithms utilized. Despite some predictions of altered splicing motifs, EX-SKIP predicted the mutant allele was unlikely to induce exon skipping. HSF predicted potential alterations of splicing due to the disruption of an SF2/ASF exonic splicing enhancer (ESE) motif in exon 7 (Figure S2). However, the impact of the predicted loss of this ESE element is unclear. This rare variant (allele frequency = 0.000025) has been reported as causative for ARRP with or without preservation of para-arteriolar RPE, and LCA8 (Clark et al., 2010; den Hollander et al., 2004; Henderson et al., 2011). Taken together, we considered both of these variants likely candidates for disease (Table S2), although the effects of these variants at the mRNA or protein level had not been demonstrated.

3.3 | Differentiation of photoreceptor progenitor cells from patient and control iPSCs

Given the *in silico* predictions of pathogenicity, we hypothesized that one or both variants might lead to alternative splicing of the *CRB1* gene, leading to a deficit in functional CRB1 protein expression. To test this hypothesis, we generated neural retinal organoids (NRO) from control iPSCs and the LEIi006-A iPSC line previously generated from proband dermal fibroblasts (Zhang et al., 2018). After 35 days of differentiation, both control (Figure 3a-d) and patient (Figure 3e-h) iPSCs produced laminated NRO resembling early optic cups. Immunostaining demonstrated the localization of retinal ganglion cells (RGCs) and amacrine cells expressing PAX6 in the center of the organoid surrounded by a dense layer of neural retinal progenitor cells (Figure 3b-c and f-g). Clusters of immature photoreceptor progenitor cells (PPCs) expressing recoverin were identified in the developing retinal progenitor cell layer (Figure 3d and h). Ultrastructural examination of NRO by transmission electron microscopy identified photoreceptor inner segments (IS) on the surface of both control (Figure 3i,k) and patient (Figure 3j,l) NRO. Junctional complexes were observed in the subapical region of PPCs from both genotypes (Figure 3i-l). Expression of *PAX6*, *RCVRN*, and *CRB1* in NRO was confirmed by qPCR analysis of day 35 NRO cDNA, using adult human retinal cDNA as a positive control (Figure 3m). All three retinal markers were upregulated in NRO and human retina compared with undifferentiated iPSC. *PAX6* was expressed at similar levels in NRO and adult human retina, while *RCVRN* expression was lower in NRO than in adult human retina, consistent with the low numbers of PPCs observed at this early time point. *CRB1* mRNA expression was increased in NRO compared with human retina. Patient NRO expressed moderately lower levels of *PAX6*, *RCVRN*, and *CRB1* than control NRO, likely reflecting a lower efficiency of NRO induction from the patient iPSC line. Together, these results demonstrate the successful generation of early-stage NRO containing an inner RGC/amacrine cell layer and an outer retinal progenitor cell layer containing clusters of immature PPCs.

3.4 | The *CRB1* c.1892A>G variant leads to exon skipping

To examine splicing of the *CRB1* gene in patient and control PPCs, we amplified partial cDNA sequences from early NRO using primers targeting exons 3-7. We detected a 0.5 kb band in patient, but not control, NRO that corresponded to a novel *CRB1* transcript lacking exon 6 (Figure 4a). Sanger sequencing of this fragment demonstrated the splicing of exon 5 to exon 7, producing an in-frame deletion in the *CRB1* coding sequence. If translated, the transcript would produce a protein with a 319-amino acid internal deletion, p.(Gly391_Arg709del). Since full-length *CRB1* cDNA sequence was not detected in this experiment due to the large size of the full-length product (1.7 kb), we performed additional PCR screening using primers targeting exon 6 and the exon 6-7 junction to determine whether *CRB1* transcripts containing exon 6 were produced from the paternal c.1892A>G allele. A single band amplified from proband NRO displayed a single "A" peak at position c.1892, indicating the product was derived from mRNA transcribed from the maternal c.2548G>A allele (Figure S3). These results indicate that the c.1892A>G variant results in the genesis of an ESS, which leads to exon 6 skipping during pre-mRNA splicing. Based on these results, we propose a new ACMGG/AMP classification (Pathogenic (ia)) for this variant (Table S2).

3.5 | The *CRB1* c.2548G>A variant is a missense mutation

Using primers targeting exons 7-8, we detected *CRB1* transcripts in both patient and control NRO. Purification and sequencing of the patient NRO PCR product revealed a heterozygous c.2548G>A signal demonstrating the presence of *CRB1* mRNA transcribed from both alleles (Figure 4b). These results indicate that *CRB1* mRNA transcripts carrying the c.2548G>A missense mutation are produced in patient retinal cells. If translated, these transcripts are predicted to produce mutant *CRB1* proteins carrying the p.Gly850Ser amino acid substitution.

4 | DISCUSSION

In this study, we used iPSC-derived NRO to demonstrate altered *CRB1* splicing in the retinal cells of a

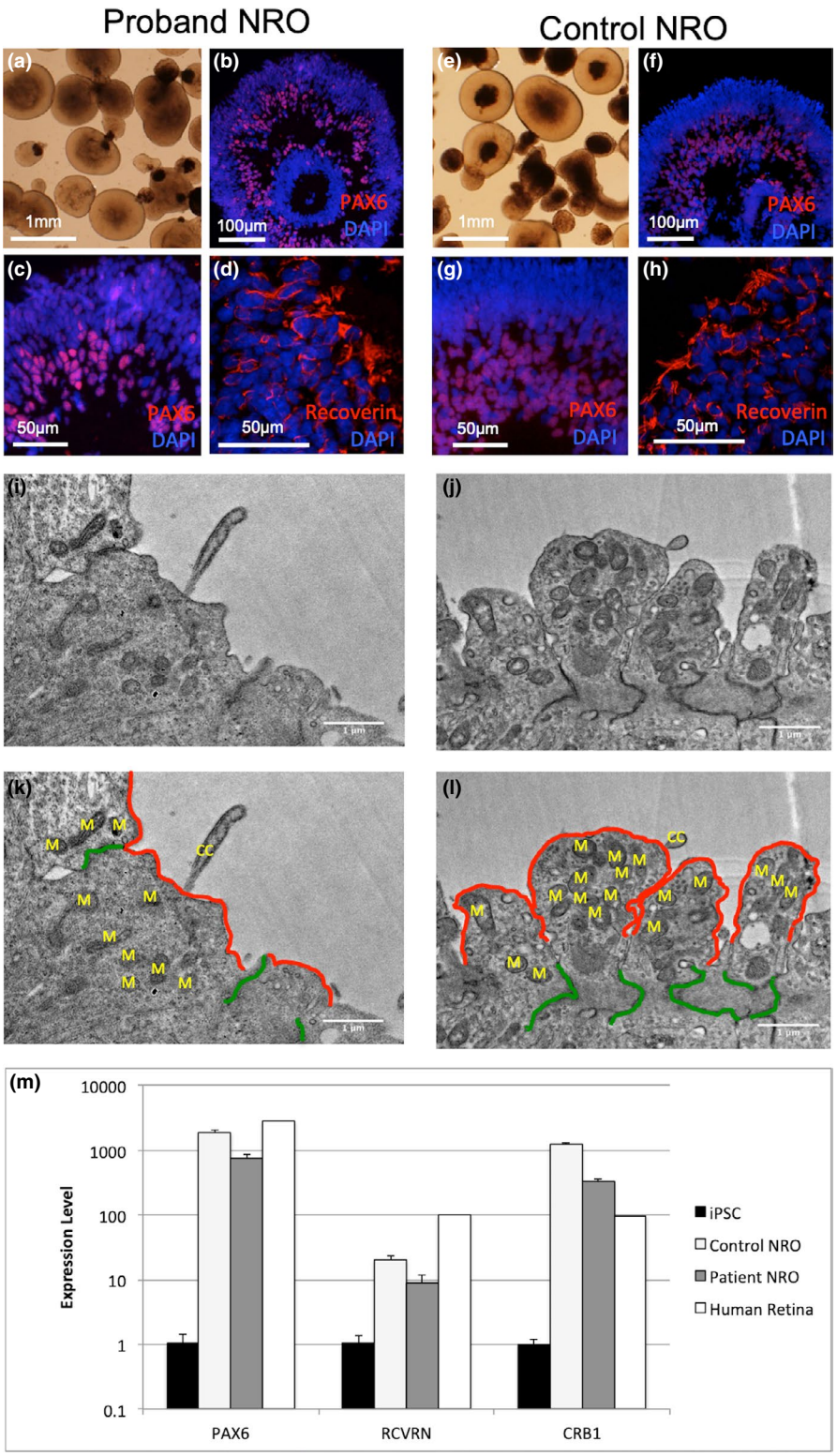

FIGURE 3 (a-h) Neural retinal organoids (NRO) were differentiated from control (a-d) and patient (e-h) iPSCs for 35 days. NRO displayed typical optic cup morphology. Immunostaining of NRO cryosections demonstrated the development of optic cup like architecture, with an inner core of PAX6 immunopositive retinal ganglion cells surrounded by a layer of retinal progenitor cells (b-c and f-g). Recoverin immunopositive cells were present in the retinal progenitor cell layer (d, h). Nuclei were counterstained with DAPI (blue signal). (i-l) Transmission electron microscopy revealed the presence of photoreceptor inner segments in both control (i) and patient (j) NRO. Lower panels (k-l) show locations of junctional complexes (green lines), the apical surface of photoreceptor inner segments (red lines), mitochondria (M) and connecting cilia (CC). Scale bars indicate 1 µm. (m) Quantitation of gene expression in NRO by qPCR demonstrated upregulation of *PAX6*, *RCVRN*, and *CRB1* expression in NRO and adult human retina, compared with undifferentiated iPSC. No significant differences in *PAX6* or *CRB1* expression were found between control and patient NRO. Bar graphs show the mean expression values normalized to LEIi005-A iPSC. Error bars indicate standard deviation.

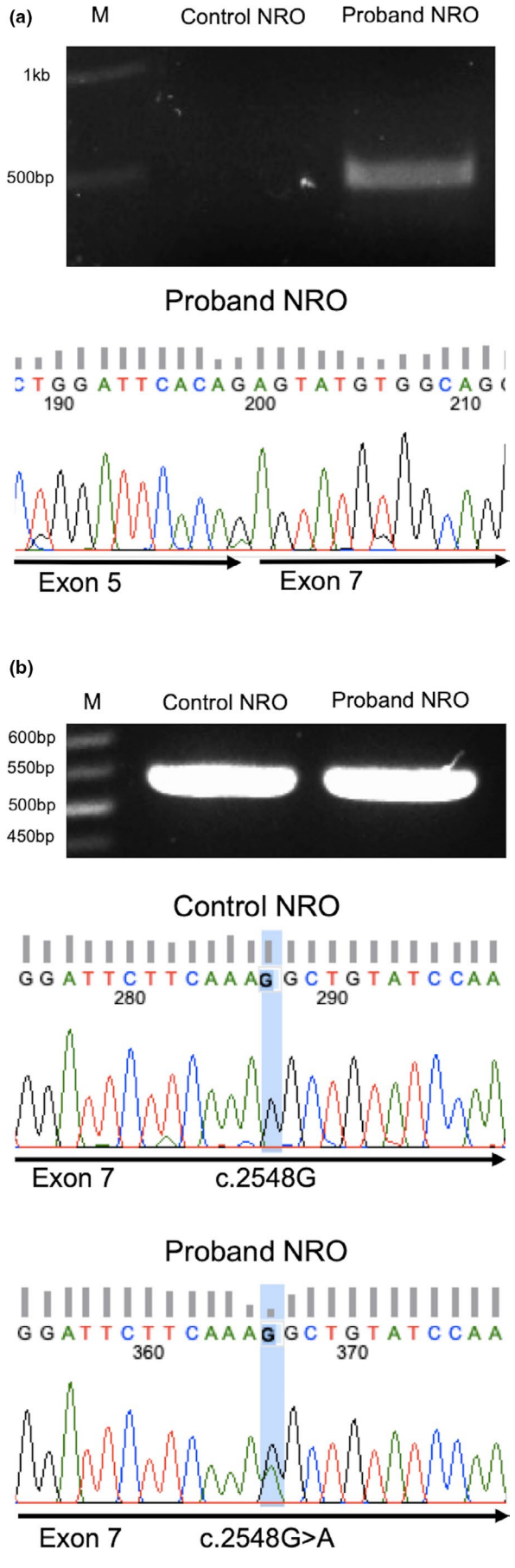

FIGURE 4 (a) Using primers to amplify exons 3-7, a 0.5 kb PCR product was detected in proband, but not in control, NRO cDNA samples. Sanger sequencing of this 0.5 kb PCR product demonstrated skipping of exon 6. (b) Using primers to amplify exons 7-8, a 0.6 kb PCR product was detected in cDNA samples from both control and proband NRO. Sanger sequencing of the PCR product detected in proband NRO demonstrated a heterozygous G/A signal at the c.2548 position, indicating the presence of transcripts from both alleles. Sizes of molecular weight markers (M) are indicated.

patient with the compound heterozygous *CRB1* mutations c.[1892A>G];[2548G>A]. The c.1892A>G variant, previously classified as a missense variant, was shown to cause exon 6 skipping, whereas the c.2548G>A variant produced *CRB1* transcripts encoding the p.Gly850Ser missense mutation. These results are supported by the clinical observation of impaired retinal maturation in OCT scans from both the proband and her affected sibling. These rare *CRB1* variants have previously been associated with severe retinal dystrophies, and are present in variation databases with clinical assertions of VUS or pathogenic. The conflicting *in silico* results for the c.1892A>G variant likely reflect the perspective of these programs, with those assessing nucleotide and amino acid substitutions considering this variant to be a neutral change. Mutation Taster, which also assesses splicing changes, utilizes NNSplice, which analyses the structure of donor and acceptor splice sites and not changes to exonic splice enhancers/silencers, explaining the benign prediction. In contrast, EX-SKIP and HSF, which take into account the ESE/ESS profile, predicted the possibility of exon skipping.

In the literature, the *CRB1* c.1892A>G variant has been associated with retinal dystrophy and ARRP (Hettinga et al., 2016; Quinn et al., 2019; Talib et al., 2017), while *CRB1* c.2548G>A has been associated with LCA8, and ARRP with or without preserved para-arteriolar RPE (Clark et al., 2010; den Hollander et al., 2004; Henderson et al., 2011). In a recent study, Quinn et al. characterized human fetal retinal tissues and iPSC-derived NRO and showed that expression of crumbs complex proteins *in vivo* was closely recapitulated by the *in vitro* human NRO model (Quinn et al., 2019). While CRB2 was abundantly detected in the subapical region of PPCs and Muller glia of first trimester and early (2 month) NRO, CRB1 immunoreactivity was sporadic and not localized to the subapical regions at these time points. CRB1 immunoreactivity and subapical localization increased with retinal maturation. Additionally, these authors characterized NRO derived from three patients with *CRB1* mutations, one of whom carried the c.1892A>G mutation. Late stage (6 month) NRO from all three patient iPSC lines displayed features previously associated with crumbs complex deficiencies in mouse models, including disrupted outer limiting membrane formation and mislocalization of photoreceptors (Quinn et al., 2019).

In the present study, we did not observe overt defects in early NRO, consistent with the limited CRB1 protein expression in early retinal development. However, since early NRO expressed *CRB1* mRNA, we were able to determine the effects of two mutations on splicing of the *CRB1* transcript. We identified putative protein-coding transcripts expressed from both alleles (Figure 4).

The allele carrying the c.2548G>A variant produced a *CRB1* transcript predicted to encode a mutant CRB1 protein incorporating a single amino acid substitution, p.(Gly850Ser). This glycine residue was previously shown to be conserved across all nine laminin A/G domains found in human *CRB1*, mouse *Crb1* and Drosophila *Crb* (den Hollander et al., 2004), suggesting a critical role in protein structure and function. Replacement of the small, uncharged glycine residue with the larger, polar serine may disrupt protein folding or interfere with the protein–protein interactions mediated by this domain.

Consistent with HSF and EX-SKIP predictions, which showed the generation of an ESS in exon 6 by the c.1892A>G variant, we also demonstrated the presence of exon 6-skipped *CRB1* transcripts in patient NRO harboring this mutation. Removal of exon 6 from the *CRB1* transcript results in an in-frame deletion of 957 bp of sequence encoding 319 amino acids that include a calcium-binding EGF-like domain, two EGF-like domains and a Laminin A/G domain (den Hollander et al., 2004). These domains play an essential role in protein–protein interactions and calcium binding (Selander-Sunnerhagen et al., 1992), suggesting the truncated protein might have reduced function. However, the presence of intact transmembrane and C-terminal domains in the mutant protein may preserve some ability to interact with other core crumbs complex proteins. Indeed, the late age of onset in the proband supports the presence of residual CRB1 function in the retina: in contrast to patients with null alleles who manifest blindness in the first year of life, our patients maintained visual function for at least the first decade.

The previous association of the c.2548G>A variant with early onset LCA suggests the missense substitution likely has a severe effect on CRB1 protein function. To date, the c.1892A>G variant has only been reported in patients with disease onset in the second to fifth decade of life, suggesting it could have a more moderate effect. Moving forward, characterization of expression, localization, and interactions of these putative mutant CRB1 proteins in late-stage NRO is required to ascertain the level of residual CRB1 function from the in-frame deletion of exon 6 and the p.(Gly850Ser) substitution.

In conclusion, our study confirmed the pathogenicity of the c.1892A>G and c.2548G>A variants in *CRB1* in a family with recessive adult-onset rod-cone dystrophy. We demonstrated the utility of patient-NRO in confirming the effects of c.1892A>G and c.2548G>A variants on transcript splicing. Future transcript analysis in *CRB1* patient-NRO may allow characterization of more exonic and intronic mutations that lead to altered splicing, thus revealing a molecular basis to explain the clinical phenotype and an opportunity for development of personalized treatment using splicing interventions.

ACKNOWLEDGMENTS

This work was funded by the Australian National Health and Medical Research Council (GNT1188694, MRF1142962, GNT1116360) and Ophthalmic Research Institute of Australia. The authors acknowledge the generous donations from the Miocevich family, Saleeba family, McCusker family, the Australian Foundation for the Prevention of Blindness and the University of Western Australia (International Postgraduate Research Scholarship). The Australian Inherited Retinal Disease Registry acknowledges the financial support of Retina Australia.

CONFLICT OF INTEREST

The authors declare that there is no conflict of interest.

AUTHOR CONTRIBUTION

SM, FKC, and XZ contributed to project design and wrote the manuscript draft. All authors contributed to data collection and analysis as well as revision and final approval of the published manuscript.

DATA AVAILABILITY STATEMENT

The data that support the findings of this study are available from the corresponding author upon reasonable request.

ORCID

Jennifer A. Thompson https://orcid.org/0000-0003-3553-6457
Samuel McLenachan https://orcid.org/0000-0001-5732-7387
Fred K. Chen https://orcid.org/0000-0003-2809-9930

REFERENCES

Adzhubei, I. A., Schmidt, S., Peshkin, L., Ramensky, V. E., Gerasimova, A., Bork, P., … Sunyaev, S. R. (2010). A method and server for predicting damaging missense mutations. *Nature Methods*, *7*(4), 248–249. https://doi.org/10.1038/nmeth0410-248

Bujakowska, K., Audo, I., Mohand-Said, S., Lancelot, M. E., Antonio, A., Germain, A., … Zeitz, C. (2012). CRB1 mutations in inherited retinal dystrophies. *Human Mutation*, *33*(2), 306–315. https://doi.org/10.1002/humu.21653

Chen, F. K., McLenachan, S., Edel, M., Da Cruz, L., Coffey, P. J., & Mackey, D. A. (2014). iPS Cells for Modelling and Treatment of Retinal Diseases. *J Clin Med*, *3*(4), 1511–1541. https://doi.org/10.3390/jcm3041511

Clark, G. R., Crowe, P., Muszynska, D., O'Prey, D., O'Neill, J., Alexander, S., … Simpson, D. A. (2010). Development of a

diagnostic genetic test for simplex and autosomal recessive retinitis pigmentosa. *Ophthalmology*, *117*(11), 2169–2177.e2163. https://doi.org/10.1016/j.ophtha.2010.02.029

den Dunnen, J. T., Dalgleish, R., Maglott, D. R., Hart, R. K., Greenblatt, M. S., McGowan-Jordan, J., … Taschner, P. E. M. (2016). HGVS recommendations for the description of sequence variants: 2016 update. *Human Mutation*, *37*(6), 564–569. https://doi.org/10.1002/humu.22981

den Hollander, A. I., Davis, J., van der Velde-Visser, S. D., Zonneveld, M. N., Pierrottet, C. O., Koenekoop, R. K., … Cremers, F. P. M. (2004). CRB1 mutation spectrum in inherited retinal dystrophies. *Human Mutation*, *24*(5), 355–369. https://doi.org/10.1002/humu.20093

Den Hollander, A. I., Ten Brink, J. B., De Kok, Y. J. M., Van den Born, L. I., Bhattacharya, S. S., Kellner, U., … Cremers, F. P. M. (2000). Mutations in a human homologue of Drosophila crumbs cause retinitis pigmentosa with preserved para-arteriolar RPE (RP12). *Investigative Ophthalmology & Visual Science*, *41*(4), S95.

Desmet, F. O., Hamroun, D., Lalande, M., Collod-Beroud, G., Claustres, M., & Beroud, C. (2009). Human Splicing Finder: an online bioinformatics tool to predict splicing signals. *Nucleic Acids Research*, *37*(9), e67. https://doi.org/10.1093/nar/gkp215

Henderson, R. H., Mackay, D. S., Li, Z., Moradi, P., Sergouniotis, P., Russell-Eggitt, I., … Moore, A. T. (2011). Phenotypic variability in patients with retinal dystrophies due to mutations in CRB1. *British Journal of Ophthalmology*, *95*(6), 811–817. https://doi.org/10.1136/bjo.2010.186882

Hettinga, Y. M., van Genderen, M. M., Wieringa, W., Ossewaarde-van Norel, J., & de Boer, J. H. (2016). Retinal dystrophy in 6 young patients who presented with intermediate uveitis. *Ophthalmology*, *123*(9), 2043–2046. https://doi.org/10.1016/j.ophtha.2016.03.046

Hollander, A. I. D., Heckenlively, J. R., van den Born, L. I., de Kok, Y. J. M., van der Velde-Visser, S. D., Kellner, U., … Cremers, F. P. M. (2001). Leber congenital amaurosis and retinitis pigmentosa with Coats-like exudative vasculopathy are associated with mutations in the crumbs homologue 1 (CRB1) gene. *American Journal of Human Genetics*, *69*(1), 198–203. https://doi.org/10.1086/321263

Ioannidis, N. M., Rothstein, J. H., Pejaver, V., Middha, S., McDonnell, S. K., Baheti, S., … Sieh, W. (2016). REVEL: An ensemble method for predicting the pathogenicity of rare missense variants. *American Journal of Human Genetics*, *99*(4), 877–885. https://doi.org/10.1016/j.ajhg.2016.08.016

Jacobson, S. G., Cideciyan, A. V., Aleman, T. S., Pianta, M. J., Sumaroka, A., Schwartz, S. B., … Stone, E. M. (2003). Crumbs homolog 1 (CRB1) mutations result in a thick human retina with abnormal lamination. *Human Molecular Genetics*, *12*(9), 1073–1078. https://doi.org/10.1093/hmg/ddg117

Jagadeesh, K. A., Wenger, A. M., Berger, M. J., Guturu, H., Stenson, P. D., Cooper, D. N., … Bejerano, G. (2016). M-CAP eliminates a majority of variants of uncertain significance in clinical exomes at high sensitivity. *Nature Genetics*, *48*(12), 1581–1586. https://doi.org/10.1038/ng.3703

Karczewski, K. J., Francioli, L. C., Tiao, G., Cummings, B. B., Alföldi, J., Wang, Q., … MacArthur, D. G. (2020). The mutational constraint spectrum quantified from variation in 141,456 humans. *Nature*, *581*(7809), 434–443. https://doi.org/10.1038/s41586-020-2308-7

Mellough, C. B., Collin, J., Khazim, M., White, K., Sernagor, E., Steel, D. H., & Lako, M. (2015). IGF-1 signaling plays an important role in the formation of three-dimensional laminated neural retina and other ocular structures from human embryonic stem cells. *Stem Cells*, *33*(8), 2416–2430. https://doi.org/10.1002/stem.2023

Mellough, C. B., Collin, J., Queen, R., Hilgen, G., Dorgau, B., Zerti, D., … Lako, M. (2019). Systematic comparison of retinal organoid differentiation from human pluripotent stem cells reveals stage specific, cell line, and methodological differences. *Stem Cells Translational Medicine*, *8*(7), 694–706. https://doi.org/10.1002/sctm.18-0267

Ng, P. C., & Henikoff, S. (2001). Predicting deleterious amino acid substitutions. *Genome Research*, *11*(5), 863–874. https://doi.org/10.1101/gr.176601

Paterson, R. L., De Roach, J. N., McLaren, T. L., Hewitt, A. W., Hoffmann, L., & Lamey, T. M. (2012). Application of a high-throughput genotyping method for loci exclusion in non-consanguineous Australian pedigrees with autosomal recessive retinitis pigmentosa. *Molecular Vision*, *18*, 2043–2052.

Quinn, P. M., Buck, T. M., Mulder, A. A., Ohonin, C., Alves, C. H., Vos, R. M., … Wijnholds, J. (2019). Human iPSC-derived retinas recapitulate the fetal CRB1 CRB2 complex formation and demonstrate that photoreceptors and muller glia are targets of AAV5. *Stem Cell Reports*, *12*(5), 906–919. https://doi.org/10.1016/j.stemcr.2019.03.002

Raponi, M., Kralovicova, J., Copson, E., Divina, P., Eccles, D., Johnson, P., … Vorechovsky, I. (2011). Prediction of single-nucleotide substitutions that result in exon skipping: identification of a splicing silencer in BRCA1 exon 6. *Human Mutation*, *32*(4), 436–444. https://doi.org/10.1002/humu.21458

Richards, S., Aziz, N., Bale, S., Bick, D., Das, S., Gastier-Foster, J., … Rehm, H. L. (2015). Standards and guidelines for the interpretation of sequence variants: a joint consensus recommendation of the American College of Medical Genetics and Genomics and the Association for Molecular Pathology. *Genetics in Medicine*, *17*(5), 405–424. https://doi.org/10.1038/gim.2015.30

Schwarz, J. M., Rodelsperger, C., Schuelke, M., & Seelow, D. (2010). MutationTaster evaluates disease-causing potential of sequence alterations. *Nat Meth*, *7*(8), 575–576. https://doi.org/10.1038/nmeth0810-575

Selander-Sunnerhagen, M., Ullner, M., Persson, E., Teleman, O., Stenflo, J., & Drakenberg, T. (1992). How an epidermal growth factor (EGF)-like domain binds calcium. High resolution NMR structure of the calcium form of the NH2-terminal EGF-like domain in coagulation factor X. *Journal of Biological Chemistry*, *267*(27), 19642–19649.

Stenson, P. D., Mort, M., Ball, E. V., Evans, K., Hayden, M., Heywood, S., … Cooper, D. N. (2017). The Human Gene Mutation Database: towards a comprehensive repository of inherited mutation data for medical research, genetic diagnosis and next-generation sequencing studies. *Human Genetics*, *136*(6), 665–677. https://doi.org/10.1007/s00439-017-1779-6

Talib, M., van Schooneveld, M. J., van Genderen, M. M., Wijnholds, J., Florijn, R. J., ten Brink, J. B., … Boon, C. J. F. (2017). Genotypic and phenotypic characteristics of CRB1-associated retinal dystrophies: A long-term follow-up study. *Ophthalmology*, *124*(6), 884–895. https://doi.org/10.1016/j.ophtha.2017.01.047

Tavtigian, S. V., Byrnes, G. B., Goldgar, D. E., & Thomas, A. (2008). Classification of rare missense substitutions, using risk surfaces, with genetic- and molecular-epidemiology applications. *Human Mutation*, *29*(11), 1342–1354. https://doi.org/10.1002/humu.20896

Zhang, X., Zhang, D., Chen, S.-C., Lamey, T., Thompson, J. A., McLaren, T., … McLenachan, S. (2018). Establishment of an induced pluripotent stem cell line from a retinitis pigmentosa patient with compound heterozygous CRB1 mutation. *Stem Cell Res*, *31*, 147–151. https://doi.org/10.1016/j.scr.2018.08.001

SUPPORTING INFORMATION

Additional supporting information may be found online in the Supporting Information section.

Fig S1-S3

Table S1-S2

How to cite this article: Zhang X, Thompson JA, Zhang D, et al. Characterization of *CRB1* splicing in retinal organoids derived from a patient with adult-onset rod-cone dystrophy caused by the c.1892A>G and c.2548G>A variants. *Molecular Genetics & Genomic Medicine*. 2020;8:e1489. https://doi.org/10.1002/mgg3.1489